A Wi-Fi Frequency Band Passive Biomedical Doppler Radar Sensor

Dongyang Tang, *Student Member, IEEE*, Victor G. Rizzi Varela, *Graduate Student Member, IEEE*, Davi V. Q. Rodrigues, *Graduate Student Member, IEEE*, Daniel Rodriguez, *Graduate Student Member, IEEE*, and Changzhi Li, *Senior Member, IEEE*

***Abstract*— In the past decades, dramatic investments and growth in wireless communication have occupied more and more radio frequency (RF) spectrum and created a shortage in the available radio spectrum. Hence, spectrum efficiency is a critical issue at the forefront of the research. Compared with conventional radar sensors, which rely on a transmitter and a receiver to detect a target, microwave passive sensing does not require a dedicated transmitter. Therefore, microwave passive sensing can have lower power and lower cost while saving the RF spectrum that is becoming limited in the modern wireless era. Since RF signals exist ubiquitously, microwave passive sensing technology has tremendous opportunities. This article proposes a passive biomedical Doppler radar sensor that operates at the Wi-Fi 2.4-GHz band to detect physiological motions of human subjects with a third-party 2.4-GHz transmitter. The proposed passive radar does not require a reference signal. It has a simple architecture with an LNA and a customized single-input diode-based mixer to maximize the down-conversion gain. Experiment results demonstrated that the proposed passive radar receiver has a voltage gain of 53.9 dB from the antenna output to the mixer output, and it can measure the respiration rate and the heart rate of a human subject successfully. The measured respiration rate and heart rate match the results from a fingertip pulse monitor and a chest band respiration monitor, respectively. Gesture detection was also demonstrated with the proposed passive radar.**

***Index Terms*— Biomedical sensor, diode-based mixer, Doppler, hand-gesture detection, passive radar, physiological motion detection, receiver, vital signs detection.**

I. Introduction

MICROWAVE passive sensing makes use of electromagnetic waves illuminated by a third-party transmitter to detect a target [1]. By comparing the direct signal from the transmitter and the reflected signal from the target of interest, the motion of the target can be detected. With the rapid growth of the Internet of Things (IoT) and satellites internet, wireless signals are ubiquitously present in the ambient air. It enables the possibility of microwave passive sensing at most places on our planet. Since microwave passive sensing does not transmit its own radio frequency (RF) signals, it inherently reduces cost and power compared with conventional radar sensors. Moreover, it provides a solution to address the interference with the wireless communication signals and improves the spectrum efficiency. The fast-growing wireless communication technologies require more and more radio spectrum and have started to affect conventional radars because of the potential interference. For example, major U.S. airlines recently warned that the new C-band 5G service could potentially interfere with the altimeter and cause a significant number of aircraft to be unusable. The automotive and consumer electronics industries have also been looking for interference mitigation approaches due to the increasing number of cars and appliances that rely on wireless devices operating at the same frequency for communication or sensing purposes. Therefore, microwave passive sensing technology has tremendous opportunities, and it has gained attention in recent decades.

Many efforts have been made to evaluate the feasibility of microwave passive sensing [2]–[14]. The prior arts have demonstrated the possibility of indoor positioning [2], human targets detection [3], [10], human activity and gesture recognition [4], [5], [8], [9], and vital sign monitoring [6], [11] using passive sensing technologies in the Wi-Fi frequency band. The existing microwave passive sensing works can be classified into two main categories based on whether additional RF receivers are needed or not.

One of the categories extracts target information from existing wireless communication devices, such as Wi-Fi access points [2], [5], [6]. One of the advantages of this category is that the transceivers in the Wi-Fi access points are synchronized, and it has the information for both the transmitted signal and the target reflected signal. However, because the Wi-Fi access points are not designed to detect targets, they do not directly provide targets' information as conventional radars do. In those works, the target detection needs to be extracted from the available data in the Wi-Fi system, such as received signal strength and channel state information.

Manuscript received 10 April 2022; revised 26 June 2022; accepted 6 July 2022. Date of publication 3 August 2022; date of current version 13 January 2023. This work was supported by National Science Foundation (NSF) under Grant ECCS-2030094 and Grant ECCS-1808613. This article is an expanded version from the IEEE Radio & Wireless Week, Las Vegas, NV, USA, 16–19 January 2022 [DOI: 10.1109/RWS53089.2022.9719929]. *(Corresponding author: Dongyang Tang.)*

The authors are with the Department of Electrical and Computer Engineering, Texas Tech University, Lubbock, TX 79409 USA (e-mail: dongyang.tang@ttu.edu; vrizziva@ttu.edu; davi.rodrigues@ttu.edu; daniel-fernando.rodriguez@ttu.edu; changzhi.li@ttu.edu).

Color versions of one or more figures in this article are available at https://doi.org/10.1109/TMTT.2022.3193408.

Digital Object Identifier 10.1109/TMTT.2022.3193408

It requires special Wi-Fi network interface cards to access the necessary data from the Wi-Fi access points and specially designed computationally intensive algorithms. While it is attractive to achieve the target detection without additional RF devices, the existing hardware and software limit the flexibility and performance of the system.

The other category of microwave passive sensing requires customized RF receivers but does not require access to any information inside the Wi-Fi access point [8]–[14]. Since the theories and algorithms used to extract the target for this category are identical to those used in conventional radars, we call it passive radars in the later sections. The mixer in a conventional radar needs two inputs: a local oscillator (LO) and an RF input. The LO signal is used as the reference signal to downconvert the RF input. The challenge for the passive radar is generating the reference signal or the LO signal for the mixer since it does not have a hardware connection to the transmitter. Two separated receivers were used to solve this problem in [8]–[10]: a reference receiver and a surveillance receiver. The authors assumed that the reference receiver contained the signal from the transmitter while the surveillance receiver included the reflected signal from the target. Passive radar with one receiver was proven to be feasible with an injection-locking oscillator [11]. Our previous work demonstrated the function of one receiver passive radar without an injection-locking oscillator [14]. However, the architecture was not optimized for low cost and maximum down-conversion gain. In this article, a passive radar is proposed for the 2.4-GHz Wi-Fi frequency band with a customized diode-based single-input mixer to maximize the down-conversion gain. The proposed architecture has a low cost because it only includes an RF gain stage, a diode-based mixer [18]–[26], and a baseband amplifier as the main components.

It is worth mentioning that the passive radar for Wi-Fi can be treated as a bistatic radar with a third-party transmitter and a customized receiver [9]. For a bistatic radar, if the target movement is perpendicular to the line of bistatic radar, it will not generate sufficient Doppler frequency. For biomedical vital signs monitoring, the chest movement for respiration and heartbeat is in all directions [27]. Therefore, the vital signs can be detected regardless of the relative location to the passive radar. Nevertheless, the placement of the passive radar plays a critical role in the strength and quality of the received signals.

The rest of this article is organized as follows. Section II explains the theory of operation for the proposed passive radar. Section III discusses the detailed design and the optimization for the down-conversion gain for the diode-based single-input mixer. The proposed architecture was manufactured on an FR-4 substrate to validate the theory and the effectiveness of the proposed architecture. The experimental results are presented in Section IV. Finally, conclusions are drawn in Section V.

II. Theory

Fig. 1 shows the block diagram of a conventional Doppler radar [15]. In a conventional Doppler radar [28], [29]: an oscillator generates the RF signal; the oscillator output is split by a power divider into two signals, one of them is amplified by a power amplifier and transmitted toward the target, the other one is sent to the LO port of the mixer; an LNA amplifies the phase-modulated signal reflected by the moving target in the receiver; the amplified signal is sent to the RF input port of the mixer; the mixer downconverts the RF input with the reference signal (LO) to the baseband signal, which carries the target information.

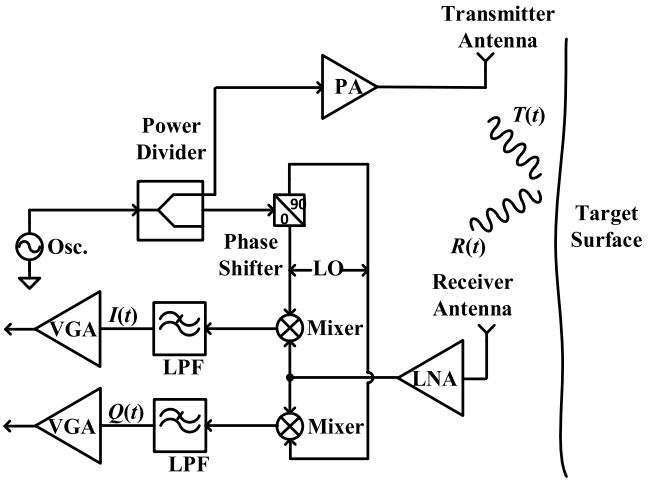

Fig. 1. Block diagram of a conventional Doppler radar.

In the proposed passive radar architecture, a third-party transmitter is responsible for transmitting the RF signal $T(t)$ to the target

$$T(t) = V_{\mathrm{TX}} \cos(2\pi f t + \varphi(t)\ ) \tag{1}$$

where f is the transmitted signal's frequency, V_{TX} is the amplitude of the transmitted signal, and $\varphi(t)$ is the phase noise of the transmitted signal. The RX antenna of the passive radar picks up the reflected signal from the target $R_1(t)$

$$R_1(t) = V_1 \cos(2\pi f(t - t_d(t)) + \varphi(t - t_d)) \tag{2}$$

where $t_d(t)$ is the time delay between the transmitted signal and the received signal, and V_1 is the amplitude of the received signal. The target's movement results in variation in the time delay and modulates the phase of the signal.

If the passive radar is on the line of sight path from the transmitter, the RX antenna also picks up the transmitted signal directly. If the receiver is not on the line of sight, static clutters will reflect the transmitted signal to the receiver, and the RX antenna will pick up the static clutter reflected signal. The received signals have a constant phase in both cases because the transmitter, the receiver, and the static clutters are all stationary. The directly received signal from the transmitter can be written as

$$R_2(t) = V_2 \cos(2\pi f t + \varphi_0 + \varphi(t - t_{d0})) \tag{3}$$

where V_2 is the received signal's amplitude, φ_0 is the constant phase shift, and t_{d0} is a constant time delay between the transmitted signal and this signal. Note that the phase noise term $\varphi(t - t_d)$ in (2) and $\varphi(t - t_{d0})$ in (3) are still correlated. Therefore, the difference between these two terms is small and negligible in short-range applications according to the range correlation theory [15], [28], [30].

It is generally true to claim that the received signal always contains the directly transmitted signal without phase modulation and the phase-modulated signal reflected from the moving target in a natural environment. If we appreciate the fact that the passive radar always receives both signals, even though both of their amplitudes can vary independently, the target can be detected by multiplying the transmitted signal with the reflected signal. Any nonlinear device can achieve the multiplication with the square term for the sum of those two signals. The proposed architecture uses a diode-based single-input mixer design since a diode has an exponential relationship between its current and voltage, which is highly nonlinear. From [16], the diode current $I(t)$ with a small-signal approximation is given in the following:

$$I(t) = I_0 + g_m(R_1(t) + R_2(t)) + \frac{g_m'}{2}(R_1(t) + R_2(t))^2 + \cdots \tag{4}$$

where I_0 is the bias current, $gm = dI/dV$ is the transconductance, and $g_m' = dI^2/d^2V$ is the second-order derivative of the current applying on the square term of the input voltage. The square term in the current is the main nonlinear contribution to multiply and downconvert the signals. The baseband output current $I_{\mathrm{BB}}(t)$ can be found by substituting (2) and (3) into the square term inside (4), and then using trigonometric identities to expand it

$$I_{\mathrm{BB}}(t) = \frac{g_m'}{2} V_1 V_2 \cos(2\pi f t_d(t) + \varphi_0). \tag{5}$$

To extract the target movement from (5), the fast Fourier transform (FFT) will be applied which is the same approach as in a conventional Doppler radar [17].

The circuit diagram for the proposed passive Doppler radar is shown in Fig. 2. The received signal is amplified by an LNA, which is implemented as two LNAs (ADL5611) cascaded to provide a 40-dB gain for microwave passive sensing applications. The LNA's output is ac coupled to a Schottky diode D_1's anode (Infineon-BAT15-02LRH) with a capacitor C_1 to isolate the output common mode of the LNA from the diode's bias voltage. The diode D_1 is used as a single-port mixer. The anode of D_1 is also connected to an inductor L_1 (Coilcraft_0603HP_R36) as an RF choke. The other side of L_1 is connected to a resistor R_1, then to the supply. R_1 needs to meet the power dissipation requirement since it carries a large current. The output of the diode-based mixer is between L_1 and R_1, and it is ac coupled to the baseband amplifier by a capacitor C_2. The cathode of D_1 is shorted to a dc ground and a radius stub which works as an ac ground at 2.4 GHz. The baseband amplifier has a low-pass filter (LPF) implemented by R_2, R_3, and C_4 for the common-mode reference to filter out the supply noise. It is also designed to have a bandpass transfer function for the input signal. The lower and upper frequencies for the passband are set by $1/(2\pi C_2 R_4)$ and $1/(2\pi C_3 R_5)$, respectively. Since the frequency range for the signal of interest is from sub-Hz to hundreds of Hz, the high-pass corner frequency is set at around 0.1 Hz to remove the dc offset at the mixer's output, and the low-pass corner frequency is set around 1 kHz and used as an antialiasing filter before digitizing the signal with an analog-to-digital converter. The dc gain of the baseband amplifier is set by the ratio of R_5 and R_4.

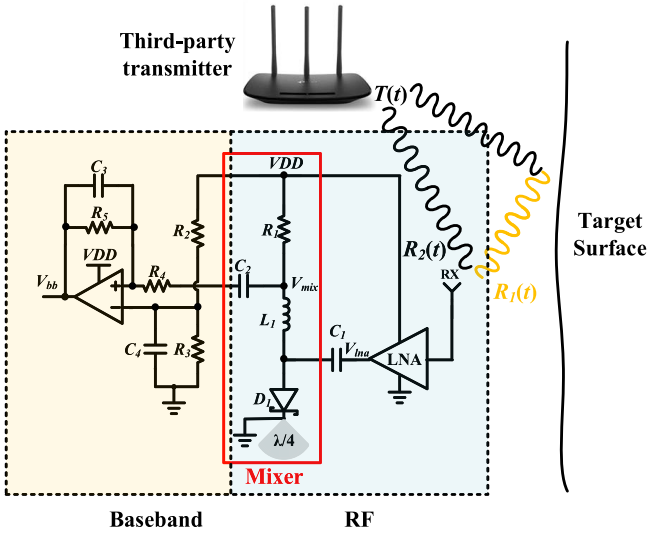

Fig. 2. Circuit diagram for the proposed passive Doppler radar.

III. Diode-Based Mixer Design

The purpose of having the RF choke L_1 is to provide a high impedance at 2.4 GHz so that the load impedance on the other side of L_1 is negligible when it is compared with the impedance of L_1 itself. The resistor R_1 is required to provide an impedance between D_1 and supply at the baseband frequency, such that the baseband current from D_1 can flow through it to generate an output voltage. Otherwise, L_1 is a short at the baseband frequency and the supply shorts directly to the anode. Since the resistance of R_1 is in parallel with the small-signal resistance of the diode, it needs to be much larger than the small-signal impedance of the diode to not affect the down-conversion gain of the diode-based mixer. Another function of R_1 is to set the bias current for the diode. Since D_1 is a Schottky diode, the voltage across the diode is approximately zero, and the bias current of the diode is approximately as $I_0 \approx \mathrm{Vdd}/R_1$. The diode I–V relationship is given by

$$\begin{aligned} I &= I_s\left(e^{\frac{qV}{nkT}} - 1\right) \\ &\approx I_s e^{\frac{qV}{nkT}} \end{aligned} \tag{6}$$

where q is the charge of an electron, k is Boltzmann's constant, T is the temperature, n is the ideality factor which typically varies from 1 to 2 based on the structure of the diode, and I_s is the saturation current. The approximation holds for $V \gg nkT/q$. From (6), the diode's small-signal resistance r_{eq} and g_m' can be calculated as follows:

$$\begin{aligned} r_{\mathrm{eq}}\big|_{I=I_0} &= \left.\frac{1}{g_m}\right|_{I=I_0} \\ &= \left.\left(\frac{dI}{dV}\right)^{-1}\right|_{I=I_0} \\ &= \frac{1}{\frac{q}{nkT} I_0} \end{aligned} \tag{7}$$

$$g'_m\big|_{I=I_0} = \left.\frac{d^2I}{dV^2}\right|_{I=I_0} = \left(\frac{q}{nkT}\right)^2 I_0. \tag{8}$$

Equations (7) and (8) show that the bias current of the diode determines both r_{eq} and g'_m, and they differ from each other just by a constant. Both of them contribute to the diode's down-conversion gain, as will be shown later.

As mentioned previously, the RF choke provides a high impedance at 2.4 GHz. Hence, the total impedance looking into the diode is mainly decided by the diode's small-signal resistance, assuming that the parasitic cap at 2.4 GHz is also negligible. Hence, the bias current of the diode also affects the input impedance matching for the mixer and indirectly affects the diode's down-conversion gain. Since r_{eq} is inversely proportional to the bias current, it drops from infinite to zero as the bias current increases from 0 to infinite. There is a bias point that makes the diode's small-signal resistance equals to the output impedance of the LNA and achieves good matching. On the other hand, the g'_m keeps increasing as the current increases. Because of this, the best bias point for the maximum down-conversion gain may not be the bias point that allows the best matching.

The previous analysis shows that all the parameters that affect the down-conversion gain are related to the bias current of the diode. Hence, a mathematic equation that relates the bias current to the down-conversion gain can be derived to provide more insight into selecting the bias current that maximizes the down-conversion gain. A small-signal model with the second-order term of the Taylor series for diode current can be developed to analyze the down-conversion gain for the single-input diode-based mixer. The proposed mixer's small-signal model is shown in Fig. 3(a). V_{LNA} is the output of the LNA, and Z_0 is 50 Ω assuming that the LNA output is matched. The circuits circled in blue are the proposed equivalent model for the diode to facilitate the calculation: r_s is the series resistance for the diode; r_{eq} is the small-signal resistance of the diode; the current source $(1/2)g'_m V^2_{\text{diode}}$ represents the nonlinear baseband current which comes from the square term of (4). The parasitic capacitance and inductance of the equivalent model are ignored here for simplicity because they are not dominant at 2.4 GHz. One should note that R_4 is drawn to be connected to a small-signal ground in the model also for simplicity. It is correct at low frequency since the baseband amplifier's inputs are virtual grounds. At high frequency, the gain of the amplifier drops to zero, and it should be treated as open. If the parasitic capacitance is considered, R_4 should be collected to the parasitic capacitance. Since R_4 can be designed to be much larger than r_{eq}, it can be ignored even if it is connected to the ground. Therefore, assuming R_4 is short to ground for all frequencies that does not affect the accuracy of the conclusion.

Since the mixer converts high-frequency RF signals to low-frequency baseband signals, the small-signal model can be simplified by analyzing the high frequency and low frequency separately. The small-signal models for high frequency and low frequency are shown in Fig. 3(b) and (c), respectively. It should be noted that the nonlinear current of the diode-based

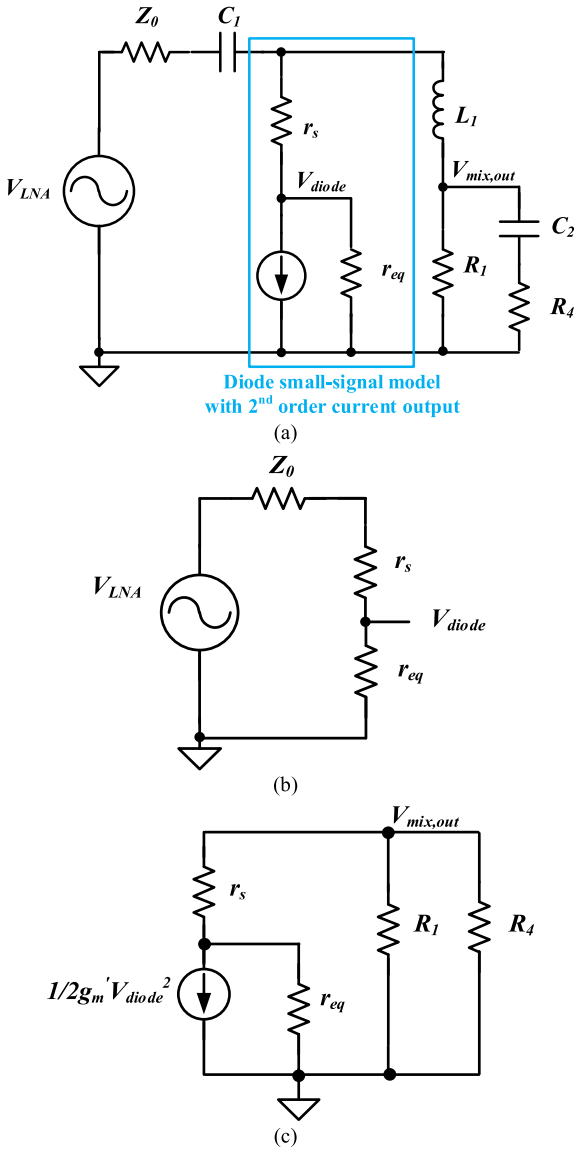

Fig. 3. Small-signal model for the diode-based mixer: (a) full model for the diode-based mixer; (b) high-frequency (RF) model for the diode-based mixer; and (c) low-frequency (baseband) model for the diode-based mixer.

mixer needs to exclude the voltage drop on the series resistance r_s, so V_{diode} is the voltage applied on the p-n junction of the diode and contributes to the down-conversion. At the high frequency (RF), C_1 and C_2 are short, L_1 is an open, and the current source $(1/2)g'_m V^2_{\text{diode}}$ is eliminated since it models the baseband current. At the low frequency (baseband frequency), C_1 is open, L_1 is short, and C_2 is designed to be short at the frequency of the interest for the baseband so that the mixer output can be ac coupled to the baseband. Note that the V_{diode} in the current source expression $(1/2)g'_m V^2_{\text{diode}}$ is the RF input voltage for the mixer, so it needs to be calculated from the high-frequency model. From Fig. 3(b), it is easy to find the actual RF input voltage to the diode V_{diode} as

$$V_{\text{diode}} = V_{\text{LNA}} * \frac{r_{\text{eq}}}{Z_0 + r_s + r_{\text{eq}}}. \tag{9}$$

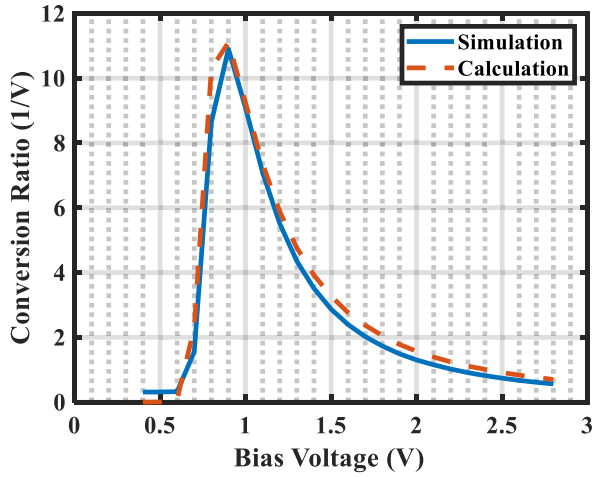

Fig. 4. Diode-based mixer's conversion ratio versus bias voltage from SPICE simulation and calculation.

From the low-frequency model, the output of the mixer $V_{\text{mix,out}}$ can be calculated with Thevenin equivalent circuit

$$V_{\text{mix,out}} = \frac{1}{2} g_m{}' V_{\text{diode}}^2 r_{\text{eq}} * \frac{R_4 // R_1}{R_4 // R_1 + r_{\text{eq}} + r_s}. \tag{10}$$

Substituting (9) into (10)

$$V_{\text{mix,out}} = \frac{1}{2} g_m' r_{\text{eq}} V_{\text{LNA}}^2 \frac{r_{\text{eq}}^2}{\left(Z_0 + r_s + r_{\text{eq}}\right)^2} * \frac{R_4 // R_1}{R_4 // R_1 + r_{\text{eq}} + r_s}. \tag{11}$$

Similar to the derivation from (4) to (5), the mixer's baseband voltage output V_{BB} can be written as

$$V_{\text{BB}} = \frac{1}{2} g_m' r_{\text{eq}} V_1 V_2 \frac{r_{\text{eq}}^2}{\left(Z_0 + r_s + r_{\text{eq}}\right)^2} * \frac{R_4 // R_1}{R_4 // R_1 + r_{\text{eq}} + r_s}. \tag{12}$$

If $R_4 \gg R_1 \gg (r_{\text{eq}} + r_s)$, substituting (7) and (8) into (12), V_{BB} can be simplified to

$$V_{\text{BB}} \approx \frac{1}{2} \frac{q}{nkT} V_1 V_2 * \frac{1}{\left(\frac{q}{nkT} I_0 (Z_0 + r_s) + 1\right)^2}. \tag{13}$$

Equation (13) indicates that the amplitude of the baseband output voltage reduces as the bias current increases. On the other hand, when the I_0 is small, $r_{\text{eq}} \gg R_4$, R_1, substituting (7) and (8) into (12) again, V_{BB} can be simplified into a different equation

$$V_{\text{BB}} \approx \frac{1}{2} \left(\frac{q}{nkT}\right)^2 I_0 V_1 V_2 (R_4 // R_1). \tag{14}$$

Equation (14) indicates that mixer output amplitude increases as the bias current increase.

The analysis above shows that an ideal bias point must exist to maximize the down-conversion gain. The down-conversion gain for the diode was simulated with a SPICE diode model to validate the analysis. Both V_1 and V_2 were set to 10 mV to approximate the small-signal condition. The baseband outputs were recorded with different bias voltages. Then, the same bias points were used to calculate the baseband output using (12).

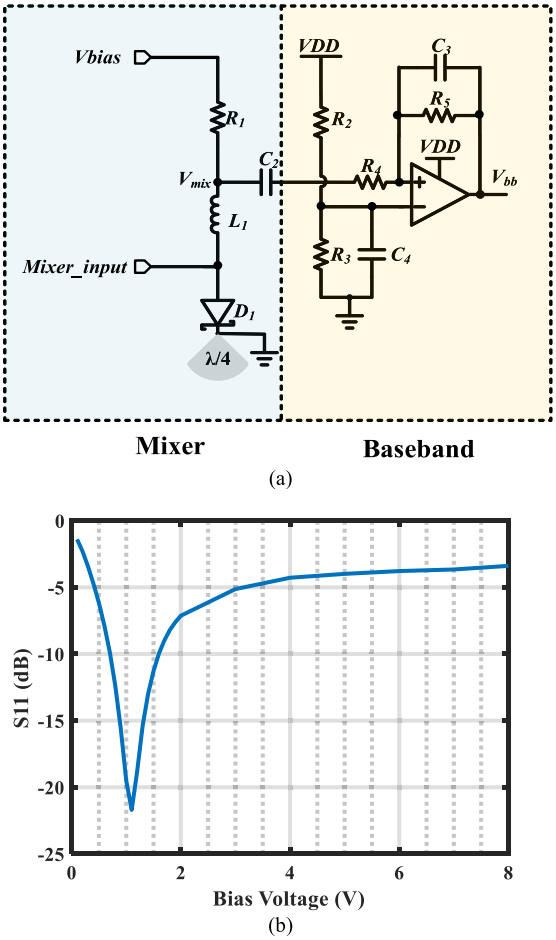

Fig. 5. (a) Circuit under test for the diode-based mixer stand-alone test. (b) S11 for the diode-based mixer versus bias voltage.

Conventionally, the down-conversion gain of a mixer is defined as $G = V_{\text{BB}}/V_{\text{RFin}}$ under a fixed LO output power. Because the baseband signal for the single-input mixer is a strong function of both input signals, it might be easier to use the conversion ratio defined as $V_{\text{BB}}/V_1/V_2$ instead of the conversion gain to analyze and compare different mixer designs. The conversion gain can be calculated from the conversion ratio by multiplying the conversion ratio with the LO voltage. Fig. 4 plots the conversion ratio as the function of the bias voltage for both simulation and calculation. The x-axis is the bias voltage in voltage, and the y-axis is the conversion ratio in $1/V$. As can be seen, the calculated conversion ratio matches closely with the SPICE model simulation.

IV. Experimental Results

In this section, the diode-based mixer was characterized stand-alone first to find out the maximum down-conversion gain, and then, the full passive radar was tested.

A. Diode-Based Mixer

The circuit under test is shown in Fig. 5(a). First, the bias voltage for the diode was swept, and the S11 of the diode was measured. Fig. 5(b) shows the results. The x-axis is the bias

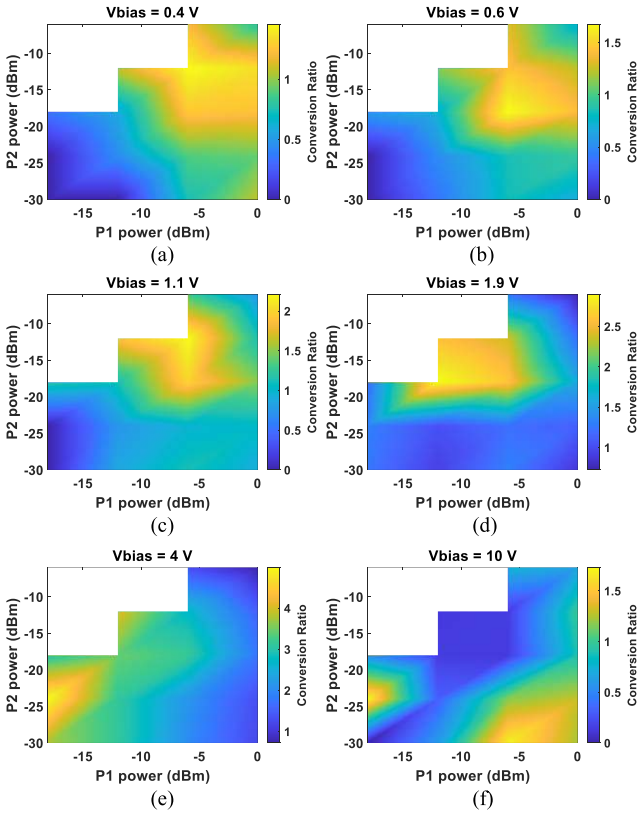

Fig. 6. Diode-based mixer's down-conversion ratio with different input power levels and different bias voltages: (a) Vbias is 0.4 V; (b) Vbias is 0.6 V; (c) Vbias is 1.1 V; (d) Vbias is 1.9 V; (e) Vbias is 4 V; and (f) Vbias is 10 V.

voltage in volts, and the y-axis is the S11 in dB. The best matching was achieved with 1.1-V bias voltage, and the S11 was -21.75 dB.

Since the maximum down-conversion gain does not necessarily coincide with a good matching based on the previous analysis, the down-conversion gain of the diode was measured with different bias points in the following experiment. In this experiment, a power combiner was used at the input of the mixer to combine two RF inputs. One RF input was set at 2.4 GHz, and another was set at 2.4 GHz plus 1-Hz offset to simulate the heartbeat's frequency. A few bias points were picked to cover both sides of the best matching point based on Fig. 5(b), and the powers of both inputs were swept independently. The baseband amplifier had a voltage gain of 40 dB, and the baseband output voltage at 1 Hz was recorded to calculate the down-conversion ratio. The results were plotted in Fig. 6(a)–(f). Each plot is for different bias voltages. The x-axis is the first input's power in dBm; the y-axis is the second input's power in dBm; and the color code represents the down-conversion ratio. The plot shows that when the bias voltage is 4 V, the down-conversion ratio is larger compared with other bias voltages across different combinations of two inputs. The maximum down-conversion ratio of 4.985, or 13.95 dB, was achieved. From Fig. 5(b), the S11 with a 4-V bias point is about -4.5 dB, which is not an outstanding good matching but is sufficient for the proposed application as the corresponding insertion loss is about 2 dB. Therefore, for the rest of the works on system demonstration, 4-V bias was used.

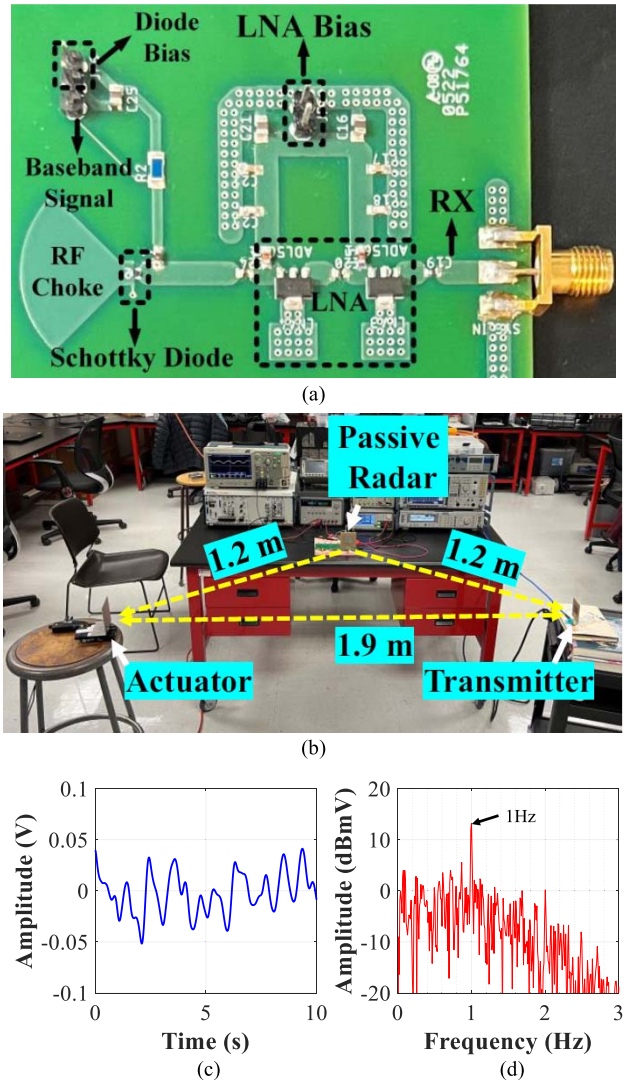

Fig. 7. Passive radar experiment with actuator as target: (a) photograph for the PCB of the proposed passive radar; (b) in laboratory setup; (c) transient waveform for the baseband output; and (d) spectrum for the baseband output.

B. Passive Radar

This section covers the experiments with the proposed passive radar. The printed circuit board (PCB) photograph for the proposed passive radar is shown in Fig. 7(a). First, an actuator carrying a metal plate (10 cm $\times$ 10 cm) was used as the target to better control the target movement and get repeatable results. The experimental setup is shown in Fig. 7(b). The distance from the transmitter to the passive radar was 1.2 m, from the transmitter to the actuator was 1.9 m, and from the passive radar to the actuator was 1.2 m. Because the maximum allowable power for Wi-Fi is 20 dBm, the power level of the transmitted signal was set to 15 dBm in this experiment. The actuator was moving periodically at 1 Hz with 0.2-mm displacement to mimic the chest movement from the human subject's heartbeat. The baseband outputs were digitized using a data acquisition device (DAQ). Fig. 7(c) shows the transient waveform for the recorded baseband output, the x-axis is the time in seconds, and the y-axis is the amplitude in volts. Fig. 7(d) shows the spectrum for the baseband output, the x-axis is the frequency in Hz, and the y-axis is the amplitude

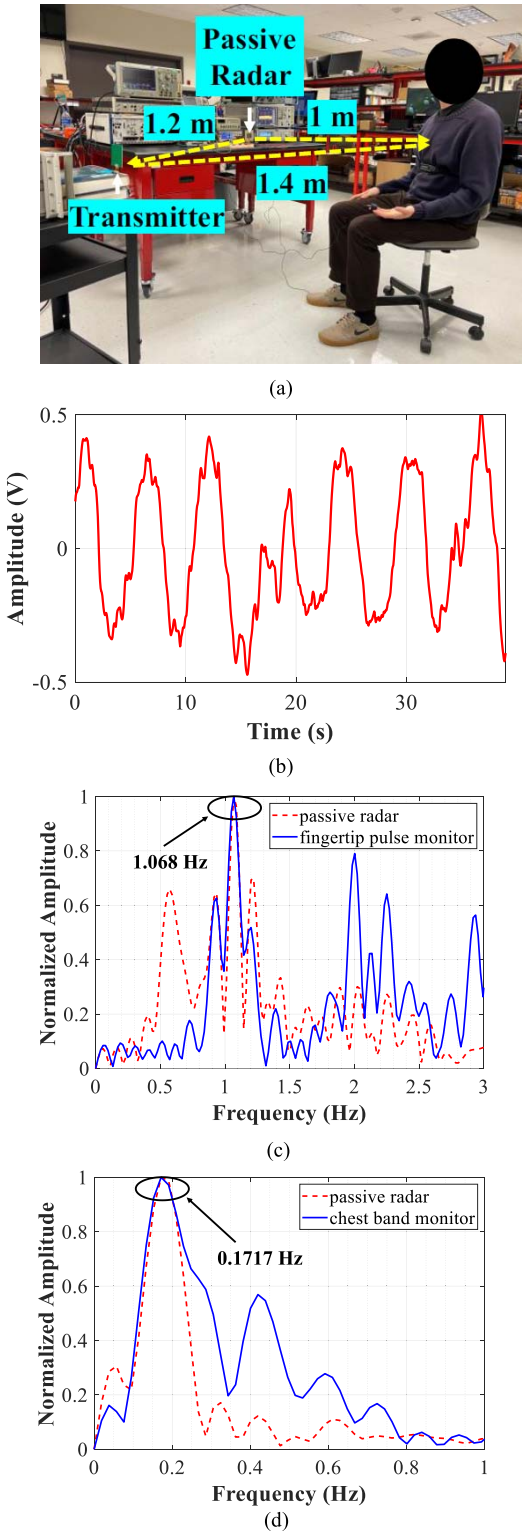

Fig. 8. Passive radar experiment with human subject: (a) in laboratory setup; (b) raw data for the passive radar baseband; (c) FFT of the high-pass filtered passive radar's output and the fingertip pulse monitor's output; and (d) FFT of the low-pass filtered passive radar's output and the chest band respiration monitor's output.

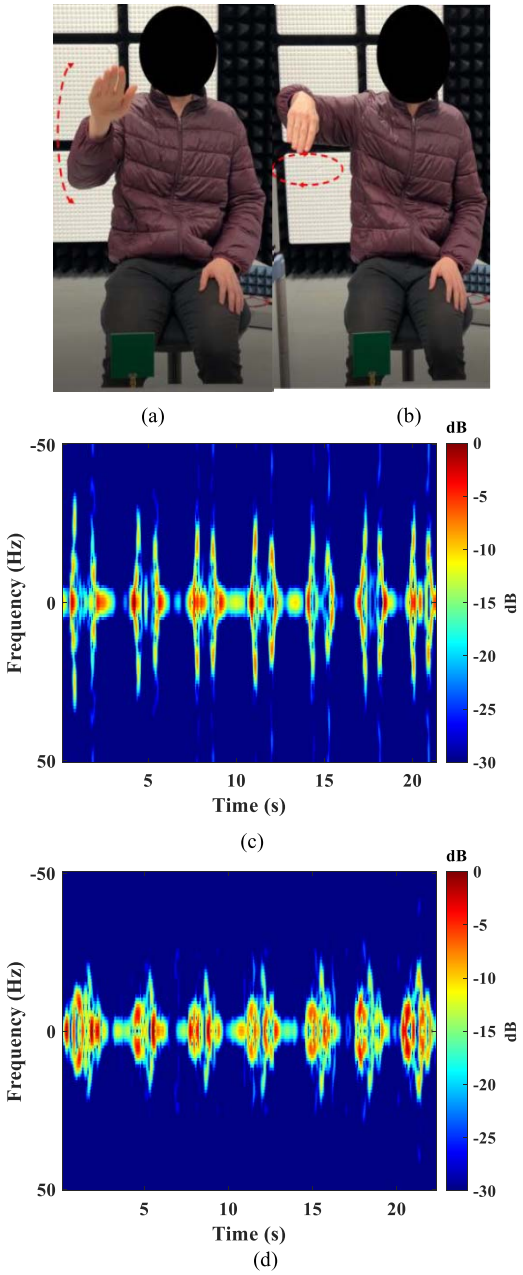

Fig. 9. Hand-gesture detection: (a) illustration for hand-click; (b) illustration for horizontal rotation of the hand; (c) spectrogram for hand-click; and (d) spectrogram for horizontal rotation of the hand.

in dBmV. A 1-Hz tone is shown in the spectrum which matches the actuator's displacement frequency.

Then, the passive radar was used to measure a human subject's respiration rate and the heart rate. Fig. 8(a) shows the experimental setup. A human subject was sitting in front of the radar. At the same time, a fingertip pulse monitor and a chest band monitor were used as the ground truth for the heart rate and respiration, respectively. The distance from the transmitter to the passive radar was 1.2 m, from the transmitter to the human subject was 1.4 m, and from the passive radar to the human subject was 1 m. The DAQ recorded the baseband output from the passive radar and the monitors' outputs for the fingertip pulse monitor and the chest band monitor. The transmitter output power was the same 15 dBm as the previous experiment. Fig. 8(b) shows the transient waveform for the passive radar's baseband output, the x-axis is the time in seconds, and the y-axis is the amplitude in volts. The digitized

baseband output was fed into two different digital filters to separate the heartbeat signals from the respiration signals. For heart rate measurement, a 0.6-Hz high-pass filter was used; for respiration rate measurement, a 0.6-Hz LPF was used. Fig. 8(c) shows the spectrum of the high-pass filtered passive radar's output and the spectrum of the fingertip pulse monitor's output for the heartbeat measurement. The x-axis is the frequency in Hz, and the y-axis is the normalized amplitude. Fig. 8(d) shows the spectrum of the low-pass filtered passive radar's output and the spectrum of the chest band respiration monitor's output, the x-axis is the frequency in Hz, and the y-axis is the normalized amplitude. It shows that the human subject's heart rate was approximately 64 beats/min, and the respiration rate was about 10.3 breaths/min. Both the heart rate and respiration rate measurement results were in agreement with the fingertip pulse monitor's result and the chest band monitor's result, respectively.

The last experiment was hand-gesture detection using micro-Doppler effects. The distance from the transmitter to the passive radar, from the transmitter to the human subject, and from the passive radar to the human subject were all 1 m. Fig. 9(a) and (b) illustrates two hand gestures from the human subject in the experiments: hand-click (moving one of the forearms from 90° to 0° with respect to the ground) and horizontal rotation of the hand. In the experiment, each gesture was repeated for seven times. Fig. 9(c) presents the Doppler spectrogram for the hand-click. It has two strips for each repetition with a similar profile. The first strip is for the forearm to move down, and the second strip is for the forearm to move back to the original position and prepare for the next repetition. Fig. 9(d) presents the Doppler spectrogram for the horizontal rotation of the hand. The frequency changes gradually from 0 to a peak and then comes back to 0 because of the circular movement.

V. Conclusion

This article proposes a low-cost passive radar with a single-input mixer based on a diode for physiological motions of human subjects. The proposed passive radar makes use of the ambient electromagnetic wave illuminated by a third-party 2.4-GHz transmitter to achieve target detection, and it does not require knowing any other information for the transmitter. A PCB prototype was fabricated with FR-4 substrate and tested in the laboratory. The experimental results demonstrated that the maximum down-conversion ratio of the designed diode-based mixer is about 13.95 dB. Vital signs sensing and hand-gesture detection were also demonstrated with a human subject to show the effectiveness of the proposed architecture.

References

[1] J. Wu, Y. Lu, and W. Dai, "Off-grid compressed sensing for WiFi-based passive radar," in *Proc. IEEE Int. Symp. Signal Process. Inf. Technol. (ISSPIT)*, Dec. 2016, pp. 258–262.

[2] C. Feng, W. S. A. Au, S. Valaee, and Z. Tan, "Received-signal-strength based indoor positioning using compressive sensing," *IEEE Trans. Mobile Comput.*, vol. 11, no. 12, pp. 1983–1993, Dec. 2012.

[3] T. Yoshida and Y. Taniguchi, "Estimating the number of people using existing WiFi access point in indoor environment," in *Proc. Eur. Conf. Comput. Sci. (ECCS)*, 2015, pp. 46–53.

[4] S. Tan and J. Yang, "WiFinger: Leveraging commodity WiFi for fine-grained finger gesture recognition," in *Proc. 17th ACM Int. Symp. Mobile Ad Hoc Netw. Comput.*, Jul. 2016, pp. 201–210.

[5] W. Wang, A. X. Liu, M. Shahzad, K. Ling, and S. Lu, "Device-free human activity recognition using commercial WiFi devices," *IEEE J. Sel. Areas Commun.*, vol. 35, no. 5, pp. 1118–1131, May 2017.

[6] X. Wang, C. Yang, and S. Mao, "PhaseBeat: Exploiting CSI phase data for vital sign monitoring with commodity WiFi devices," in *Proc. IEEE 37th Int. Conf. Distrib. Comput. Syst. (ICDCS)*, Jun. 2017, pp. 1230–1239.

[7] Y. Ma, G. Zhou, and S. Wang, "WiFi sensing with channel state information: A survey," *ACM Comput. Surv.*, vol. 52, no. 3, p. 46, Jul. 2019.

[8] W. Li, B. Tan, and R. Piechocki, "Passive radar for opportunistic monitoring in e-Health applications," *IEEE J. Transl. Eng. Health Med.*, vol. 6, pp. 1–10, 2018.

[9] K. Chetty, G. E. Smith, and K. Woodbridge, "Through-the-wall sensing of personnel using passive bistatic WiFi radar at standoff distances," *IEEE Trans. Geosci. Remote Sens.*, vol. 50, no. 4, pp. 1218–1226, Apr. 2012.

[10] Y.-C. Lai, C.-C. Chou, M.-C. Tang, T.-S. Horng, and F.-K. Wang, "Finger gesture sensing and recognition using a Wi-Fi-based passive radar," in *IEEE MTT-S Int. Microw. Symp. Dig.*, Jun. 2019, pp. 293–296.

[11] M.-C. Tang, F.-K. Wang, and T.-S. Horng, "Vital-sign detection based on a passive WiFi radar," in *IEEE MTT-S Int. Microw. Symp. Dig.*, Sep. 2015, pp. 74–75.

[12] M.-C. Tang, F.-K. Wang, and T.-S. Horng, "Human gesture sensor using ambient wireless signals based on passive radar technology," in *IEEE MTT-S Int. Microw. Symp. Dig.*, May 2015, pp. 1–4, doi: 10.1109/MWSYM.2015.7167080.

[13] F.-K. Wang, M.-C. Tang, Y.-C. Chiu, and T.-S. Horng, "Gesture sensing using retransmitted wireless communication signals based on Doppler radar technology," *IEEE Trans. Microw. Theory Techn.*, vol. 63, no. 12, pp. 4592–4602, Sep. 2015.

[14] D. V. Q. Rodrigues, D. Tang, and C. Li, "A novel microwave architecture for passive sensing applications," in *Proc. IEEE Radio Wireless Symp. (RWS)*, Jan. 2022, pp. 57–59.

[15] D. Tang, J. Wang, W. Hu, Z. Peng, Y.-C. Chiang, and C. Li, "A DC-coupled high dynamic range biomedical radar sensor with fast-settling analog DC offset cancelation," *IEEE Trans. Instrum. Meas.*, vol. 68, no. 5, pp. 1441–1450, May 2019.

[16] D. M. Pozar, *Microwave Engineering*, 4th ed. Hoboken, NJ, USA: Wiley, 2011.

[17] C. Li, V. M. Lubecke, O. Boric-Lubecke, and J. Lin, "A review on recent advances in Doppler radar sensors for noncontact healthcare monitoring," *IEEE Trans. Microw. Theory Techn.*, vol. 61, no. 5, pp. 2046–2060, May 2013.

[18] M. R. Barber, "Noise figure and conversion loss of the Schottky barrier mixer diode," *IEEE Trans. Microw. Theory Techn.*, vol. MTT-15, no. 11, pp. 629–635, Nov. 1967.

[19] G. Kühnle, H. Mayer, H. Olbrich, W. Steffens, and H.-C. Swoboda, "Low-cost long-range radar for future driver assistance systems," *Auto Technol.*, vol. 3, no. 4, pp. 76–80, Jul. 2003.

[20] V. Issakov, H. Knapp, M. Wojnowski, A. Thiede, and W. Simbuerger, "A 22–39 GHz passive mixer in SiGe:C bipolar technology," in *IEEE MTT-S Int. Microw. Symp. Dig.*, May 2010, pp. 1012–1015.

[21] I. Maestrojuan, I. Ederra, and R. Gonzalo, "Fourth-harmonic Schottky diode mixer development at sub-millimeter frequencies," *IEEE Trans. Terahertz Sci. Technol.*, vol. 5, no. 3, pp. 518–520, May 2015.

[22] E. Ozturk *et al.*, "A 120 GHz SiGe BiCMOS monostatic transceiver for radar applications," in *Proc. 13th Eur. Microw. Integr. Circuits Conf. (EuMIC)*, Sep. 2018, pp. 41–44.

[23] D. Rodriguez and C. Li, "A low-power and low-cost monostatic radar based on a novel 2-port transceiver chain," in *Proc. IEEE Top. Conf. Wireless Sensors Sensor Netw. (WiSNeT)*, Jan. 2020, pp. 9–12.

[24] B. Sene, H. Knapp, D. Reiter, and N. Pohl, "A compact monostatic transceiver topology using a diode-based mixer," in *Proc. IEEE 20th Top. Meeting Silicon Monolithic Integr. Circuits RF Syst. (SiRF)*, Jan. 2021, pp. 7–10.

[25] B. Sene, D. Reiter, H. Knapp, and N. Pohl, "Design of a cost-efficient monostatic radar sensor with antenna on chip and lens in package," *IEEE Trans. Microw. Theory Techn.*, vol. 70, no. 1, pp. 502–512, Jan. 2022.

[26] B. Sene, D. Reiter, H. Knapp, and N. Pohl, "From gunnplexer to MMIC: An implementation on a single chip," *IEEE Microw. Mag.*, vol. 23, no. 1, pp. 48–53, Jan. 2022.

[27] C. Li, Y. Xiao, and J. Lin, "Experiment and spectral analysis of a low-power Ka-band heartbeat detector measuring from four sides of a human body," *IEEE Trans. Microw. Theory Techn.*, vol. 54, no. 12, pp. 4464–4471, Dec. 2006.
[28] A. D. Droitcour, O. Boric-Lubecke, V. M. Lubecke, J. Lin, and G. T. A. Kovacs, "Range correlation and I/Q performance benefits in single-chip silicon Doppler radars for noncontact cardiopulmonary monitoring," *IEEE Trans. Microw. Theory Techn.*, vol. 52, no. 3, pp. 838–848, Mar. 2004.
[29] H.-C. Kuo *et al.*, "A fully integrated 60-GHz CMOS direct-conversion Doppler radar RF sensor with clutter canceller for single-antenna non-contact human vital-signs detection," *IEEE Trans. Microw. Theory Techn.*, vol. 64, no. 4, pp. 1018–1028, Apr. 2016.
[30] M. C. Budge and M. P. Burt, "Range correlation effects on phase and amplitude noise," in *Proc. Southeastcon*, Apr. 1993, p. 5.

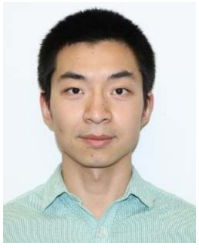

Dongyang Tang (Student Member, IEEE) received the B.Sc. degree in microelectronics from Sichuan University, Chengdu, China, in 2011, the M.Sc. degree in electrical engineering from the University of Michigan, Ann Arbor, MI, USA, in 2013, and the Ph.D. degree in electrical engineering from Texas Tech University, Lubbock, TX, USA, in 2022.

He joined Qualcomm, San Diego, CA, USA, in 2013, as a Mixed-Signal IC Design Engineer, where he is currently a Staff Engineer with the Qualcomm MSIC Group. His research interests include mixed-signal integrated circuit and system, and RF integrated circuits and systems.

Victor G. Rizzi Varela (Graduate Student Member, IEEE) received the B.S. degree in electronics and telecommunications engineering from Mackenzie Presbyterian University, São Paulo, Brazil, in 2019. He is currently pursuing the Ph.D. degree in electrical engineering at Texas Tech University, Lubbock, TX, USA.

He joined Texas Tech University, in 2021, as a Research Assistant. His current research interests include biomedical applications of microwave/RF, microwave/millimeter-wave circuits and systems, and wireless sensors.

Davi V. Q. Rodrigues (Graduate Student Member, IEEE) received the B.S. degree in communications engineering from the Military Institute of Engineering, Rio de Janeiro, Brazil, in 2017. He is currently pursuing the Ph.D. degree in electrical engineering at Texas Tech University, Lubbock, TX, USA.

From 2009 to 2011, he was with the Brazilian Navy. He became a member of the Brazilian Army in 2013 and was commissioned as First Lieutenant of the Military Engineers Branch in 2017. In 2018, he served in the Southern Military Command, Porto Alegre, Rio Grande do Sul, Brazil. He joined Texas Tech University, in 2018, as a Research Assistant. In 2021, he was with Uhnder, Inc., Austin, TX, where he was involved in the design and evaluation of signal processing algorithms for the mitigation of radar interference. In 2022, he was with the Abbott Laboratories, Los Angeles, CA, USA, where he was involved in the design of antennas and microwave systems for next-generation implantable medical devices. His research interests include structural health monitoring based on Doppler radars, wireless sensors for smart living and biomedical applications, and microwave/millimeter-wave circuits and systems.

Mr. Rodrigues was a recipient of the Best Student Paper Award of the 2020 IEEE MTT-S International Microwave Biomedical Conference (IMBioC), the Best Paper Award—Antennas Category of the 2020 IEEE MTT-S Asia–Pacific Microwave Conference (APMC), the Best Student Paper Award—Honorable Mention of the 2021 IEEE MTT-S International Wireless Symposium (IWS), the First Prize Award of the IEEE MTT-S IMS Adaptive Relay Transceiver Design Competition in 2019, the Second Prize Award of the IEEE MTT-S IMS High-Sensitivity Motion Radar Design Competition in 2019 and 2021, the IEEE MTT-S Graduate Fellowship Award, and the prestigious IEEE MTT-S Tom Brazil Graduate Fellowship Award in 2022. He was a finalist of the Student Paper Contest at the 2021 IEEE MTT-S Radio Wireless Week (RWW).

Daniel Rodriguez (Graduate Student Member, IEEE) received the B.S. degree in electronics and telecommunication engineering from the Universidad Autonoma del Caribe, Barranquilla, Colombia, in 2014, and the Ph.D. degree in electrical engineering from Texas Tech University, Lubbock, TX, USA, in 2022.

He is currently an Analog Engineer with Intel Corporation, Hillsboro, OR, USA. His research interests are radar systems, microwave/millimeter-wave sensing, and microwave circuits.

Dr. Rodriguez was awarded as an HSF Scholar in 2019. He received the IEEE MTT-S Graduate Fellowship Award in 2020 and the JT and Margaret Talkington Graduate Fellowship in 2017. He is an Active Reviewer for the IEEE TRANSACTIONS ON MICROWAVE THEORY AND TECHNIQUES, the IEEE JOURNAL OF ELECTROMAGNETICS, RF AND MICROWAVES IN MEDICINE AND BIOLOGY, and the IEEE SENSORS JOURNAL.

Changzhi Li (Senior Member, IEEE) received the B.S. degree in electrical engineering from Zhejiang University, Hangzhou, China, in 2004, and the Ph.D. degree in electrical engineering from the University of Florida, Gainesville, FL, USA, in 2009.

He is currently a Professor with Texas Tech University, Lubbock, TX, USA. His research interests are microwave/millimeter-wave sensing for healthcare, security, energy efficiency, structural monitoring, and human–machine interface.

Dr. Li is the IEEE Microwave Theory and Techniques Society (MTT-S) Distinguished Microwave Lecturer, Tatsuo Itoh Class of 2022–2024. He was a recipient of the IEEE MTT-S Outstanding Young Engineer Award, the IEEE Sensors Council Early Career Technical Achievement Award, the ASEE Frederick Emmons Terman Award, the IEEE-HKN Outstanding Young Professional Award, the NSF Faculty Early CAREER Award, and the IEEE MTT-S Graduate Fellowship Award. He is an Associate Editor of the IEEE TRANSACTIONS ON MICROWAVE THEORY AND TECHNIQUES and the IEEE JOURNAL OF ELECTROMAGNETICS, RF AND MICROWAVES IN MEDICINE AND BIOLOGY.